Experimental Investigation on Eliminating Supercooling Nature of Ice and Improving its Energy Storage Performance to Establish an Energy-Efficient Cold Thermal Storage

Solaimalai Raja Rakkappan[a], Suresh Sivan[a]*, Hongwei Wu[b], Srinivasan L[a], Thejeshwar Karthikeyan[a]

[a] Nanotechnology Research Laboratory, National Institute of Technology, Tiruchirappalli – 620015, Tamil Nadu, India.

[b]School of Physics, Engineering and Computer Science, University of Hertfordshire, Hatfield, AL10 9AB, United Kingdom

*Corresponding author Email: ssuresh@nitt.edu

Abstract

Energy efficiency is a crucial parameter for sustainable development. Eliminating the supercooling and enhancing the energy storage performance of the ice-cold thermal storage system (CTSS) is vital to make it more reliable and sustainable. In the present study, the supercooling issue of ice was eliminated using 1-Hexadecanol. Further, the energy storage performance of ice was enhanced using an aluminium honeycomb core (AHC), which is considered to be the most promising method of improving the charging performance. The optimal size of AHC was identified by performing the experiments with three sizes (large, medium and small) of AHC. Further, the discharging [heat transfer fluid temperature (T_w) = 13 °C)] and the charging [T_w = -3, -6 and -9 °C)] experiments were conducted before and after adding the optimal size AHC inside the various diameters (64, 85 and 105 mm) spherical enclosure (S.E)). The supercooling nature of water is eliminated after adding 3 wt% of 1-Hexadecanol, and the medium-size AHC is optimal. The optimum heat transfer fluid temperature for charging is -6 °C, and the smallest diameter S.E provided better discharging and charging performance. The average decrease in charging time and improvement in charging rate realised upon adding AHC are 30.23% and 43.54%, respectively. When the AHC is added with ice, the effective utilisation ratio improved considerably (6.13 to 6.48), and the energy storage capacity reduced slightly (1.76% to 1.91%). The above experimental results implicate that the employment of AHC would pave the way for effectively enhancing the energy storage performance of ice.

Keywords: Supercooling; Charging; Nucleating Agent; 1-Hexadecanol; Aluminium Honeycomb Core

Nomenclature

a_{hex}	Hexagonal cell parameter, Å
$c_{p_{\mathrm{AHC}}}$	Specific heat of AHC J g^{-1} K^{-1}
$c_{p_{1-\mathrm{Hex}}}$	Specific heat of 1-Hexadecanol, J g^{-1} K^{-1}
$c_{p_{\mathrm{ice}}}$	Specific heat of ice, J g^{-1} K^{-1}
$c_{p_{wa}}$	Specific heat of water, J g^{-1} K^{-1}
CR	Charging rate, W
CT	Charging time, min
Dia	The outer diameter of S.E, mm
DR	Discharging rate, W
DT	Discharging time, min
$E_{\mathrm{AHC+1-Hex}}$	Energy recovered/stored in AHC and 1-Hexadecanol, J
E_{wa}	Energy recovered/stored in water, J
ΔH_{wa}	Enthalpy of freezing of water, J g^{-1}
k	Thermal conductivity, W m^{-1} K^{-1}
m_{AHC}	Mass of AHC in S.E, g
m_{1-Hex}	Mass of 1-Hexadecanol in S.E, g
m_{wa}	Mass of water in S.E, g
$\mathrm{P_n}$	Nucleation probability, -
Q_{cha}	Time-averaged charging rate J s^{-1} or W
Q_{dis}	Time-averaged discharging rate, J s^{-1} or W
t_{cha}	Charging time, seconds
t_{dis}	Discharging time, seconds
T_{i}	Initial temperature for charging time, ℃
T_{final}	Final temperature for charging time, ℃
$T_{\mathrm{p_{wa}}}$	Phase change temperature of the water, ℃
T_{w}	Heat Transfer Fluid Temperature, ℃
vol%	Volume percentage, %
wt%	Weight percentage, %

Abbreviations

AHC	Aluminium Honeycomb Core

CTSS	Cold thermal storage system
PCM	Phase change material
RTD	Resistance Temperature Detector
S.E	Spherical Enclosure
TCE	Thermal Conductivity Enhancer

1. Introduction

Due to rapid urbanisation and the growth of metro cities, air-conditioning systems usage increased remarkably [1]. It takes up a substantial share (40-50%) of overall electricity consumption in a building [2]. Hence, relocating the segment of air-conditioning system load from peak hours to off-peak hours would minimise the problem of electric load imbalance. In addition, the air-conditioning system can be designed at a lower cooling load [3], which ultimately reduces the size of an air-conditioning system and enhances the energy efficacy of the chiller, as it makes the chiller run at the intended load most of the time. The portion of peak hours air-conditioning system load can be effectively transferred to off-peak hours by integrating the cold thermal storage system (CTSS) [4].

The cold energy can be stored in CTSS by running the chiller using cheaper off-peak electricity, which can then be utilised at peak hours to run the air-conditioning system [5]. As a consequence of this, the peak-hour electricity load of an air-conditioning system could be transferred to off-peak hours, which subsequently balances the electric load imbalance [6] and reduces high Kilo-volt-ampere charges (energy cost) [4]. This also improves the operating efficiency of an air-conditioning system, as the chiller operates during the night (lower condensing temperature) [7]. CTSS uses a sensible heat system or latent heat system. However, the latent heat system offers high energy storage capacity due to phase change [8,9]. Therefore, latent heat-based CTSS has superior advantages compared to sensible heat systems [10]. The phase transition from solid to liquid and vice versa is widely preferred to store energy in CTSS [8].

Mostly ice is used as a phase change material (PCM) in a latent heat system-based CTSS. However, the chiller needs to be functioned at a lower evaporator temperature to make the ice, owing to its low freezing temperature and severe supercooling nature [11,12]. As a consequence, the coefficient of performance of the chiller decreases [13], which eventually declines the energy storage efficiency of CTSS. Therefore, to effectively utilise the ice for CTSS, the supercooling nature of water needs to be mitigated, especially in a spherical enclosure (S.E). The advantages of

using an S.E for CTSS include its favourable heat transfer characteristics [14] and ease of stacking in a storage container by ensuring adequate porosity [15]. Moreover, 50% mass is available within the 20% radius. Thus, the present study intends to investigate ice discharging/charging characteristics in an S.E.

The studies performed on minimising the supercooling nature of water are presented in our previous research [16]. It was mentioned that the supercooling could not be reduced reliably using nanoparticles because of sedimentation issues [14,17], and it cannot be mitigated entirely using nanoparticles as its crystal structure is not similar to water. Meanwhile, the supercooling issue was eliminated in a reliable and practically feasible way (no stability issue) using silver iodide (no external process is required to maintain stability, like pseudomonas and nanoparticles). However, it is not economically viable, as the price of silver iodide is substantially high (Rs. 220/g).

In our previous research [16], the supercooling issue was mitigated in a reliable and practically feasible way using 1-Decanol (long-chain fatty alcohol). However, the cost of 1-Decanol is slightly high (Rs.2.05/g). As economic viability is one of the vital parameters for any practical application, reducing the cost of nucleating agents further paves the way for establishing a cost-effective CTSS. Hence the present study aims to mitigate the supercooling issue of ice using cost-effective long-chain fatty alcohols. In this study, the 1-Hexadecanol (Cetyl Alcohol) has been identified as a promising low-cost long-chain fatty alcohol, as its cost (Rs.1.00/g) is 51.22% lower than that of 1-Decanol (the price of 1-Hexadecanol is lower than that of all the other long-chain fatty alcohols). Also, it can act as an effective nucleating agent for water like 1-Decanol, as it belongs to the family of long-chain fatty alcohols and has a crystal structure similar to water. Silver iodide, 1-Decanol and 1-Hexadecanol cost details have been taken from Loba Chemie, Mumbai, India.

Eliminating the supercooling issue of ice improves the energy efficiency of the CTSS to some extent. However, energy efficiency is a crucial parameter for sustainable development. Therefore, enhancing the charging performance of an ice-based CTSS would further improve the energy storage efficiency of CTSS. This additionally helps in establishing energy-efficient and sustainable CTSS. Thus, the present study intends to improve the charging performance of ice.

Further, the studies on improving the charging characteristics of ice using nanoparticles as a thermal conductivity enhancer (TCE) were discussed in our previous research [16]. The condition of PCM in CTSS is stable. Consequently, the settlement problem is unavoidable for nanoparticles-

based TCE [14,17]. This implies that the nanoparticles are unreliable in enhancing thermal conductivity, which hinders their usage in CTSS applications. Meanwhile, the carbon-based powder porous materials (Expanded graphite (EG)) and metal structure-based porous materials (nickel, aluminium and copper) have better characteristics to act as effective TCE [18,19], as it does not have sedimentation issues and their crucial results and their features are listed in **Table 1**.

Table 1 Various aspects of porous TCEs

S. No	PCM/TCE	Type of capsule/ Density of MF (kg m^{-3})	In a specified storage volume M.M.P.C.A/ A.M.P.A/M.M.A (g)	Reduction in C.T / Reduction in ESC (%)	E.U.R
1.	Paraffin/EG [20]	Cylindrical/NM	78.5/64.89/7.21*	NM/17.34	-
2.	Ice/EG [21]	Sphere/NM	~203.00/150.00/47.00*	80.00/26.10	3.35
3.	RT82/Copper MF [22]	Rectangular / 8950	37.10/35.30/26.20*	56.47/5.39	1.32
4.	Paraffin/EG [23]	Rectangular/NM	NM	NM/30.00	-
5.	Stearic Acid/ Copper MF [24]	Rectangular/ 8920	NM	50.00/2.70	-
6.	RT44HC/Copper MF [17]	Cylindrical / 8950	~66.68/65.00/21.50*	24.01-25.58/2.52	1.03
7.	Paraffin/Copper MF [25]	Rectangular/ 8920	NM	33.33/3.30	-
8.	Paraffin/Nichel MF [26]	Rectangular/ 8900	~76.90/75.20/19.74*	NM/2.21	-
9.	Paraffin/Aluminium MF [27]	Cylindrical/2700	73.00/69.20/14.04*	NM/5.18	-
10.	Paraffin/Aluminium MF [28]	Rectangular/2700	9.10/8.31/2.34*	NM/8.66	-
11.	RT35HC/Copper MF [29]	Cylindrical/8960	286.00/262.00/250.00*	NM/8.39	-
12.	RT82/Copper MF [30]	Rectangular/8960	77.00/73.15/44.80*	~47.65/5.00	1.30

13.	Water/AHC [P.S]	Sphere/2730	99.76/98.00/4.79	30.19/1.76	6.48
			240.80/236.32/12.24	30.18/1.86	6.13
			460.10/451.31/24.00	32.30/1.91	6.40

TCE - Thermal conductivity enhancer, M.F – Metal foam, NM - Not mentioned, A.M.P.A - Actual mass of PCM added, AHC – Aluminium Honeycomb core, C.T – Charging time, M.M.P.C.A – Maximum mass of PCM can be added, M.M.A – Mass of metal foam added, ESC - Energy Storage capacity, EG – Expanded graphite, P.S – Present Study, E.U.R - Effective utilisation ratio (ratio of % of the decrease in C.T divided by wt.% of TCE), *Calculated based on the data available in the literature.

The energy storage features of porous TCEs have been presented in **Table 2** (calculated with respect to the data illustrated in **Table 1**). **Table 2** shows that Aluminium honeycomb core (AHC) possesses superior energy storage features [31], such as a higher effective utilisation ratio for a specified cost (2.79-2.95), smaller wt% of AHC required (4.66% to 5.05%), and a lower decrease in energy storage capacity (1.76% to 1.91%) compared to other porous TCEs, as presented in **Table 2**. Thus, it is substantiated that AHC is the best and the most efficacious TCE. Hence, in this study, AHC has been used to improve ice charging characteristics.

Table 2 Energy storage aspects of porous TCEs

Porous TCE	W.P.M.R (%)	E.U.R	Cost ($)/kg [32]	R.E.S.C (%)	E.U.R/Cost ($)
High Density (Copper)	21.00 - 48.82	1.03 - 1.32	7.36	2.21 - 8.39	0.14 - 0.18
Medium Density (AHC)	4.66 - 5.05	6.13 - 6.48	2.20	1.76 - 1.91	2.79 - 2.95
EG	10.00 - 23.85	3.35	1.93	17.34 - 30.00	1.74

R.E.S.C – Reduction in Energy Storage Capacity, E.U.R – Effective utilisation ratio, W.P.M.R – wt% of porous materials required.

The significance and the originality of the current study are as follows.

- The scientific originality of the present study relies on eliminating the supercooling nature of ice (using a cost-effective nucleating agent) together with enhancing the charging characteristics of ice in a highly reliable (long-term reliability) and practically feasible (no sedimentation issue) way using AHC, which is a new exploration. It is much essential to establish an energy-efficient and sustainable CTSS.

- The novelty of the current research relied on the complete mitigation of supercooling nature of water using 1-Hexadecanol. As a result, the water freezes at 0 °C with no delay in the onset of solidification, which reduces the chiller operating time and power consumption.
- This is the first study on improving the charging characteristics of ice using an AHC (most propitious TCE compared to other TCEs (**Table 2**)). AHC has a high surface-to-volume ratio and good reliability. The inclusion of AHC leads to a 30.23% reduction in chiller operating time, leading to a 30.23% reduction in power consumption to store the stated amount of energy.
- The scientific relevance of the present research is ascribed to the advantages of using 1-Hexadecanol + AHC (as per **Table 2** data), which are:
    - ✓ Both 1-Hexadecanol (Rs.1.00/g) and AHC (for a specified cost, the effective utilisation ratio is high (2.79 to 2.95)) are cost-effective.
    - ✓ AHC has a high surface-to-volume ratio, and it can be effectively filled in S.E
    - ✓ Complete mitigation of supercooling,
    - ✓ Higher effective utilisation ratio (6.13 to 6.48)
    - ✓ Lower decrease in energy storage capacity (1.76% to 1.91%),
    - ✓ Both 1-Hexadecanol and AHC have good practical applicability and long term-reliability (no settlement issue),
- Apart from the above, a detailed experimental investigation was performed. Based on the obtained results, all the optimal parameters (optimal size of AHC, suitable diameter and optimal heat transfer fluid temperature) needed for establishing the CTSS have been discovered.

In this study, supercooling nature of ice has been eliminated using the cost-effective nucleating agent (1-Hexadecanol). Further, the charging and discharging characteristics of water + 1-Hexadecanol have been studied with and without adding various sizes (large, medium and small) of AHC in a 64 mm S.E, and the optimal size AHC has been found. The experiments were then performed using the optimal size. Further, the charging and discharging characteristics of water + 1-Hexadecanol were analysed in three different diameters S.E (outer diameter = 64, 85 and 105 mm) before and after adding AHC. The discharging studies were conducted at T_w = 13 °C, and the charging experiments were performed at T_w = -3, -6 and -9 °C. The influence of heat transfer fluid temperature on the charging characteristics of water + 1-Hexadecanol was

investigated after adding AHC. Moreover, the impact of the size of S.E on discharging and charging characteristics of water + 1-Hexadecanol has been explored with AHC.

2. Materials and methods

2.1. Materials

B.S.Innovation (Dharam Industries), New Delhi, India, supplied the AHC (Al 3003 alloy). Spectrum Reagent Chemical, Edyar, Cochin provided demineralised water. Loba Chemie Mumbai, India, supplied Cetyl Alcohol or 1-Hexadecanol ($C_{16}H_{34}O$, 242.44 g/mol, 98% Purity, 0.818 g cm^{-3}). A resistance temperature detector (RTD, class A accuracy) was obtained from the Electrical and Electronics Corporation of India, Mumbai. S.Es were provided by Borosil Limited, Mumbai, India. Chemicals were used without further purification except for 1-Hexadecanol, which is converted to crystal form from flakes.

2.2. Properties of materials used

Table 3 Properties of materials used

S.No	Properties	Value	Reference
1.	*k* of water, water + large, medium, and small size AHC (W m^{-1} K^{-1}) at 25 °C	0.60, 0.64, 0.67 and 0.69	Measured in this study
2.	*k* of ice, ice + large, medium, and small size AHC (W m^{-1} K^{-1}) at -5 °C	2.20, 2.45, 2.96 and 3.11	
3.	Specific heat of ice and water (J g^{-1} $°C^{-1}$)	2.11 and 4.18	[33] and [34]
4.	Melting and freezing point of water (°C)	0 & 0	-
5.	Freezing and melting enthalpy of ice (J g^{-1})	333.00 & 333.00	[34]
6.	Density of AHC (kg m^{-3})	2730.00	Taken from the NIST database
7.	Specific heat of 1-Hexadecanol (J g^{-1} $°C^{-1}$)	1.74	
8.	*k* of AHC (W m^{-1} K^{-1})	180.00	
9.	Specific heat of AHC (J g^{-1} $°C^{-1}$)	0.893	

Thermal conductivity (*k*) of water/ice and water/ice added with AHC (large, medium and small) were measured using a KD2 Pro thermal analyser. The measurement was done by filling the water or water + AHC in a cylindrical enclosure, and the KS-1 needle was positioned at its centre. Then three times (auto mode), the thermal conductivity study was conducted at 25 °C, and

the mean value was estimated. Similarly, a thermal conductivity study on ice or ice + AHC was performed at -5 °C with the help of a TR-1 needle. The detailed procedure can be found in [35]. The property values of materials utilised in the current study are presented in **Table 3**.

2.3. Experimentation

The charging and discharging characteristics of water + 1-Hexadecanol+ AHC have been studied using the experimental setup illustrated in **Fig. 1**. The details of the experimental setup can be found in our previous research [5]. The S.Es were filled with (Water + 1-Hexadecanol) / (AHC + Water + 1-Hexadecanol) up to 86 vol% to maintain adequate space for volume expansion of ice (Volume expansion of ice is 9 vol%, extra 5 vol% space has been provided to avoid the breakage of S.E).

Table 4 AHC-related data

Type of AHC	Thickness × Height × Core Size (mm)	Volume of 64 mm S.E & vol% filled (ml)	Mass of AHC in 64 mm (g)/volume occupied by AHC (ml)	Mass of PCM/1-Hexadecanol added (g)
Small	0.05 × 6.4 × 6.4	116.00 & ~86 vol%	5.38/1.97	95.06/2.94
Medium	0.05 × 9.5 × 9.5		4.79/1.76	95.06/2.94
Large	0.05 × 12.7 × 12.7		2.99/1.10	95.06/2.94
Without	-		-	95.06/2.94

In the current study, various sizes of AHC (large, medium, and small) have been utilised to improve the charging and discharging characteristics. The specifications of AHC have been presented in **Table 4**. Further, the AHC was added in a step-by-step manner to find the mass of AHC that can be contained in an S.E. Between the steps, S.E was shaken (rotationally) for proper containment of AHC. After adding the AHC until the neck (100 vol%), it was unpacked from S.E and weighed. With the help of this, the mass of AHC that can be added up to 86 vol% was calculated and given in **Table 4**. The mass of water, 1-Hexadecanol and AHC filled inside S.E is given in **Table 4** and **Table 7**. To compare the results logically, for a particular diameter of S.E, the mass of water + 1-Hexadecanol added was kept constant before and after adding AHC.

Furthermore, the round bottom flask made up of borosilicate glass S.E (thickness = ~1 mm) has been used in this study to visualise the phase transition process (melting & freezing) appropriately and to make the required arrangement [5,16,36–38] for the experiments (fixing the temperature sensor, filling the AHC & PCM and submerging the S.E inside the bath). In the

upcoming sections, water + 1-Hexadecanol is denoted as PCM. The 64, 85 and 105 mm S.Es containing PCM + Medium size AHC are shown in **Fig. 2**. The experimental procedure for conducting the charging and discharging characteristics can be found in [5,16,38]. In a typical air-conditioning system, the chilled water temperature entering the chiller or CTSS is 13 °C. Hence, the discharging experiments were performed at 13 °C without performing the optimisation study. All the experiments conducted with AHC have been repeated thrice, and the repeatability of the results has been confirmed.

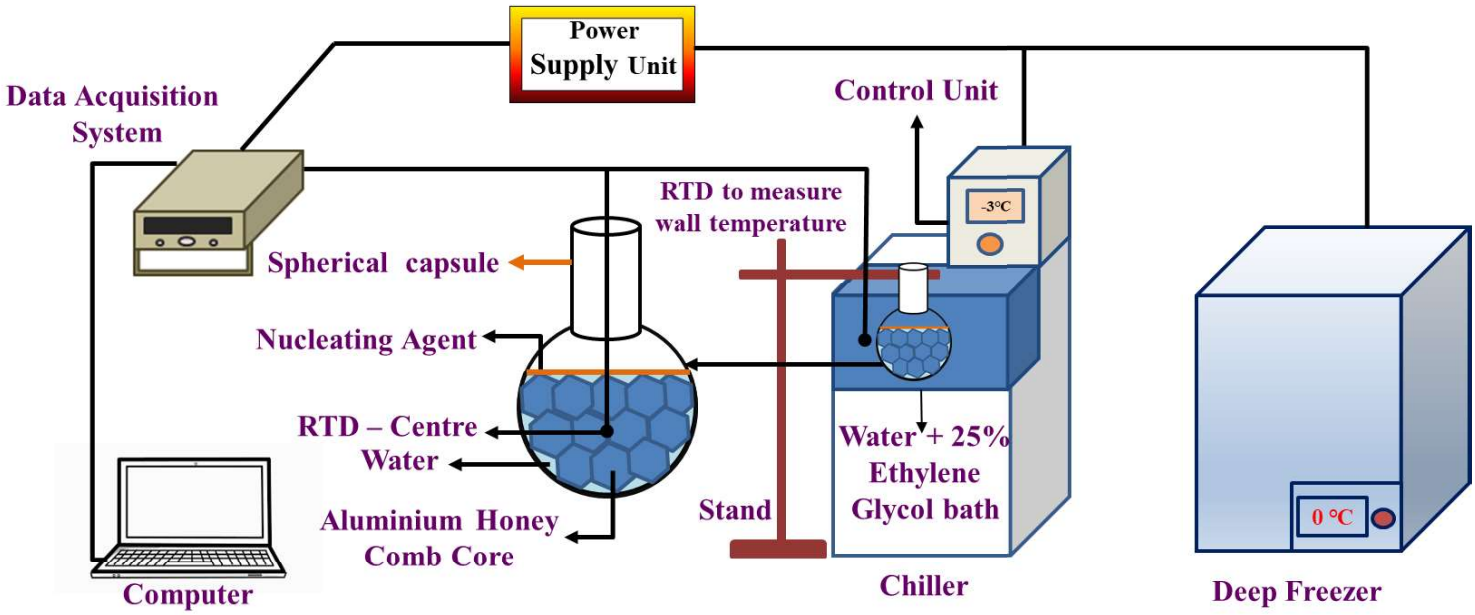

Fig. 1 Experimental (schematic) set up to explore the charging characteristics and discharging characteristics of water + 1-Hexadecanol with and without AHC.

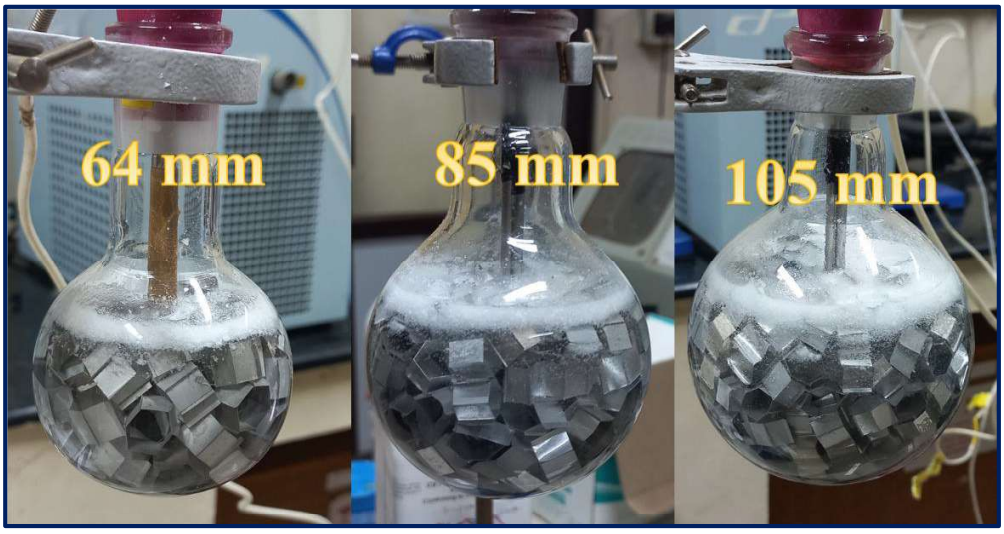

Fig. 2 Medium size AHC filled in a 64, 85, and 105 mm S.Es

2.4. Data Reduction

The amount of cold energy recovered/stored in ice was calculated using Eq.**(1)**.

$$E_{\mathrm{wa}} = \left(m_{\mathrm{wa}} c_{p_{wa}} \left|(T_{\mathrm{i}} - T_{\mathrm{p_{wa}}})\right|\right) + (m_{\mathrm{wa}} \Delta H_{\mathrm{wa}}) + \left(m_{\mathrm{wa}} c_{p_{\mathrm{ice}}} \left|(T_{\mathrm{p_{wa}}} - T_{\mathrm{final}})\right|\right) \quad \textbf{(1)}$$

The sensible heat stored in AHC and 1-Hexadecanol was calculated using Eq.**(2)**.

$$E_{\mathrm{AHC+1-Hex}} = \left(m_{\mathrm{AHC}} c_{p_{\mathrm{AHC}}} \left|(T_{\mathrm{i}} - T_{\mathrm{final}})\right|\right) + \left(m_{1-Hex} c_{p_{1-Hex}} \left|(T_{\mathrm{i}} - T_{\mathrm{final}})\right|\right) \quad \textbf{(2)}$$

The time-averaged discharging rate (DR)/charging rate (CR) was calculated using Eq.**(3)**

$$Q_{\mathrm{cha}}\ or\ Q_{\mathrm{dis}} = \frac{E_{\mathrm{wa}} + E_{\mathrm{AHC+1-Hex}}}{t_{\mathrm{cha}}\ or\ t_{\mathrm{dis}}} \quad \textbf{(3)}$$

Charging time (CT) was estimated from 7 to -1 °C, and discharging time (DT) was calculated from -1 to 7 °C.

2.5. Uncertainty

The law of propagation of error scheme was used to determine the uncertainty of various properties. The acquired uncertainty values are illustrated in **Table 5**.

Table 5 Uncertainty of properties [5]

Property measured	Uncertainty	Equipment used
Mass of Water, 1-Hexadecanol and AHC	± 2 mg	Digital weighing balance
Thermal conductivity before melting	± 10%	KD2 Pro (TR-1 needle)
Temperature of water	± 1.41 °C	Data logger and RTD
Thermal conductivity after melting	± 5%	KD2 Pro (KS-1 needle)
CR and DR	± 3.50%	-

3. Results and discussion

3.1. Suitable wt% of nucleating agent and the concept behind the elimination of supercooling

To find the suitable wt% of 1-Hexadecanol required to mitigate the supercooling, the experiments have been performed by adding different wt% of 1-Hexadecanol in a 64 mm S.E at

T_w = -3 °C. The experiment started with 0.5 wt% of 1-Hexadecanol (crystal form) present on the surface of the water, as shown in **Fig. 3** (b), and then it was increased at a step of 0.5. Each wt% was subjected to ten experiments, and the results obtained at the 10th experiment were plotted in **Fig. 3 (a).** The obtained results are plotted in **Fig. 3** (a). It is found that the supercooling was realised at 0.50, 1.00, 1.50, 2.00, and 2.50 wt% of 1-Hexadecanol. Meanwhile, at 3.00 wt% of 1-Hexadecanol, the supercooling was eliminated. Hence, 3 wt% is found as a suitable concentration of 1-Hexadecanol to eliminate the supercooling. Further experiments have been performed with 3 wt% of 1-Hexadecanol, as adding nucleating higher than 3 wt% is unnecessary to induce nucleation without supercooling, as mentioned in our previous research for 1-Decanol [16].

Further, S.E filled with water + 1-Hexadecanol is shown in **Fig. 3** (b) left image**.** After adding water + 3 wt% 1-Hexadecanol inside S.E, due to low density, 1-Hexadecanol floats over the surface of the water and forms heterogeneous nucleation sites for water. After keeping S.E containing water + 1-Hexadecanol inside the chiller, the water temperature starts to reduce. Once the temperature reaches 0 °C, the water is nucleated with the help of heterogeneous nucleation sites. The crystallisation spikes developed in an S.E during the freezing process in the presence of heterogeneous nucleation sites can be seen in **Fig. 3** (b) left image. Different stages (from initial crystallisation to complete ice formation) involved in freezing water using long-chain fatty alcohol as a nucleation agent were explained in detail in our previous research [16]. **Fig. 3** (b) right image shows S.E with the complete ice formation.

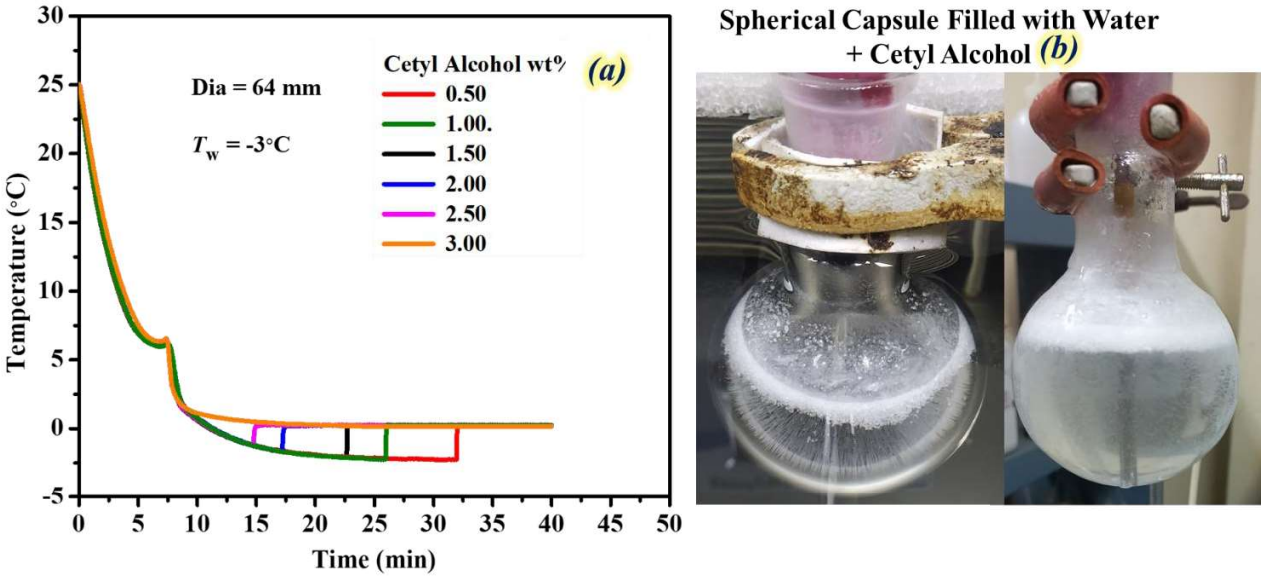

Fig. 3 (a) Suitable concentration of 1-Hexadecanol to eliminate the supercooling, (b) S.E filled with water and 1-Hexadecanol

The concept behind the elimination of supercooling using 1-Hexadecanol is an exciting phenomenon. It is intriguing to note that the intermolecular bonded O-H bond is available in both 1-Hexadecanol and water between the wavelength of 3200 to 3550 cm-1, as confirmed by **Fig. 4** (a). Details related to other peaks that emerged in 1-Hexadecanol (long-chain fatty alcohol group) were clearly explained in our previous research [16,39]. After adding 1-Hexadecanol to water, an intermolecular bonded O-H group of 1-Hexadecanol on the water's surface forms a two-dimensional hexagonal crystal lattice structure identical to a hexagonal ice structure [40]. Thus, the crystals of 1-Hexadecanol can provide a heterogeneous nucleation site for water [41,42]. The cell parameter of the two-dimensional hexagonal crystal structure of 1-Hexadecanol is $a_{\mathrm{hex}} =$ 4.72 Å [43], and it has structural similarity to the cell parameter of hexagonal ice structure, which is a_{hex} = 4.50 Å (**Fig. 4 (b) and (c)**). The crystal structure similarity [43] between 1-Hexadecanol (a_{hex}= 4.72 Å) and ice (a_{hex} = 4.50 Å) vanishes the nucleation-free energy barrier possessed by the water. As a result, the water can convert its phase to ice without supercooling [42]. The concept mentioned above is the fundamental reason for eliminating the supercooling nature of water using 1-Hexadecanol.

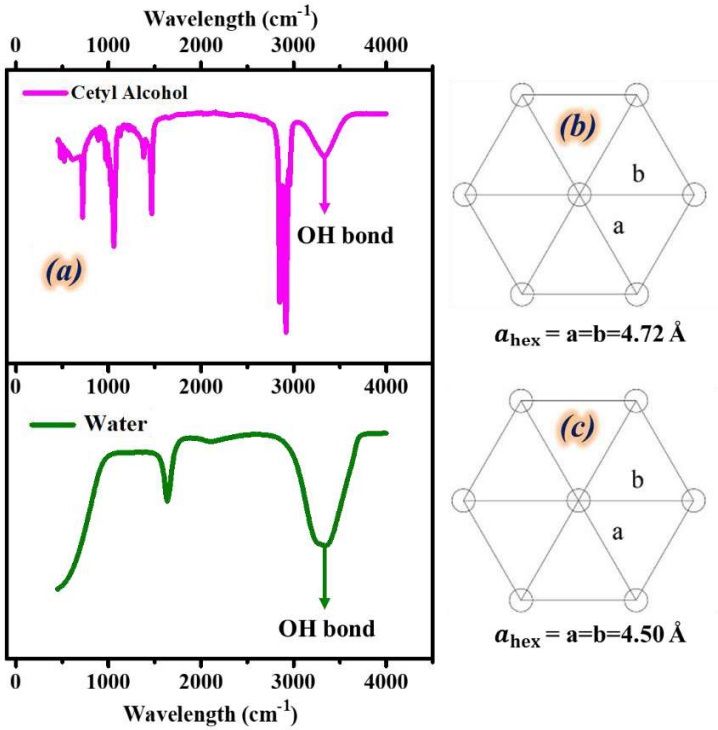

Fig. 4 (a) FTIR results of 1-Hexadecanol and water (b) Two-dimensional hexagonal crystal structure of (b) 1-Hexadecanol and (c) ice

As mentioned in [16], the long-chain fatty alcohols are immiscible in water, and their density is lower than that of water. Due to this, the 1-Hexadecanol floats on the surface of the water, as shown in **Fig. 3** (b) left image. It will remain on top regardless of the number of charging and discharging cycles and will supply nucleation sites for the water. In addition, unlike nanoparticles and pseudomonas, it does not demand external processes to preserve stability. Since 1-Hexadecanol is immiscible, it does not affect the thermal properties of water. As a result, the proposed strategy for eliminating water's supercooling characteristic is cost-effective and practically feasible, which can be effectively used to establish the economically viable CTSS. Further, the differential scanning calorimetry study is not essential to understand the freezing behaviour of water on a macro scale; the reasons for that were clearly explained in previous research [16,44–47].

3.2. Charging behaviour of ice with and without a nucleating agent

The charging behaviour of water has been studied with and without a nucleating agent. As suggested in [11,12,16], due to the probable and sporadic ice nucleation behaviour, to understand its charging performance for every heat transfer fluid temperature (T_w = -3, -6 and -9 °C), ten trials have been conducted in a 64 mm S.E. The acquired temperature-time history readings are plotted in **Fig. 5** (a) and (b). Without a nucleating agent, the experiments were stopped either after crystallisation or at 120 min. With the nucleating agent, the experiments were performed for 40 min to ensure that the crystallisation occurred without supercooling. Without a nucleating agent (**Fig. 5** (a)), it was found that at T_w = -3 °C for all the experiments, the water could not change its phase to ice even after operating the chiller for 120 min. Hence, nucleation probability (P_n) is zero, and the energy stored via latent heat is zero at T_w = -3 °C. Nucleation probability is the ratio of the number of times nucleation occurs divided by the total number of experiments conducted.

Moreover, **Fig. 5** (a) reveals that at T_w = -6 °C, for four experiments (P_n = 0.6), the water could not change its phase to ice, and for the remaining experiments, crystallisation was initiated. However, the delay in onset crystallisation time is random, which are 9.50, 12.95, 23.50, 34.82, 42.41, and 78.20 min, respectively. The delay in onset crystallisation time observed in previous studies is presented in **Table 6**. It is confirmed that while freezing the water without a nucleating agent, the delay in the onset of crystallisation is unavoidable. To vanish the ice nucleation-free energy barrier possessed by the water, the chiller desires to function at a specific duration, which would be the reason for realising delay in onset crystallisation time, as stated in [16]. Further, at T_w = -9 °C, the crystallisation is initiated for all the experiments (P_n = 1), and in two experiments, crystallisation occurred without supercooling. For the experiments in which the solidification

occurs with supercooling, the delay in onset crystallisation time is random, which are 8.80, 17.35, 11.10, 13.25, 17.80, 18.45, 26.55 and 47.25 min, respectively. The probability in water nucleation is defined as probable nucleation behaviour. The randomness in onset crystallisation time is defined as sporadic nucleation behaviour. The above results substantiate that due to supercooling nature and probable and sporadic nucleation behaviour of ice, the chiller should run ineffectively for a certain period or at a lower evaporator temperature (< -9 °C) to initiate the crystallisation. Due to the above, the chiller performance would be immensely affected, further reducing the energy storage performance of CTSS. Therefore, to efficiently utilise the ice in CTSS, the aforementioned unfavourable ice behaviours need to be mitigated, as mentioned in [11,12,16].

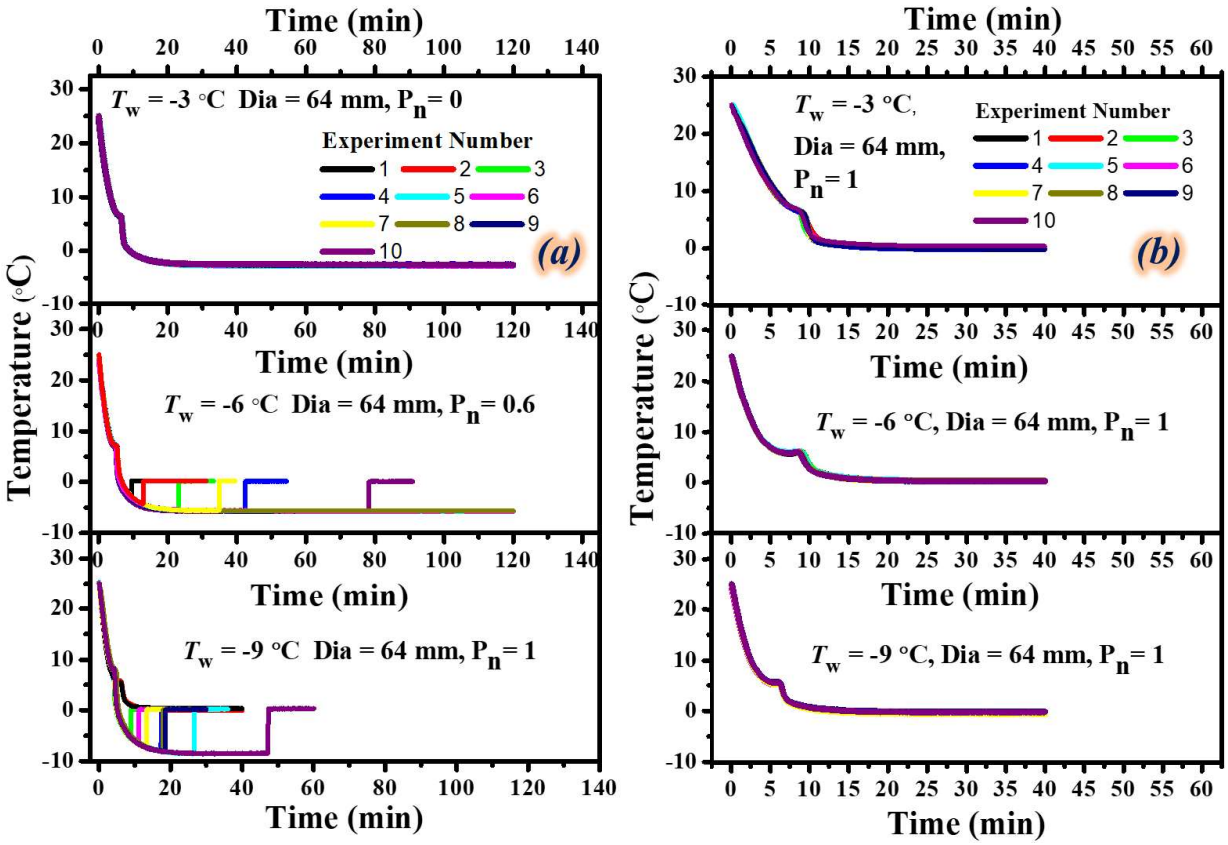

Fig. 5 (a) Freezing behaviour of water (a) without and (b) with a nucleating agent

In the present study, 1-Hexadecanol has been used as a nucleating agent, which is cost-effective and has good practical applicability, as mentioned earlier. After adding 3 wt% of 1-Hexadecanol, the supercooling nature and probable and sporadic nucleation behaviour have been mitigated in all the experiments, as confirmed from **Fig. 5** (b). By virtue of this, the crystallisation was initiated without supercooling. This further eliminates the idle running time of the chiller, which subsequently reduces the operating time required by the chiller to store the given amount of energy. Also, it lays the foundation for running the chiller at a higher evaporator temperature.

Hence, the chiller energy can be utilised effectively, which aids in achieving better energy storage efficiency, thereby paving the way for establishing sustainable CTSS. The fundamental concept behind the mitigation of supercooling has been explained in section 3.1. Different stages (from initial crystallisation to complete ice formation) involved in freezing water using long-chain fatty alcohol as a nucleating agent were described in detail in our previous research [16].

Fig. 5 (a) and (b) show two temperature plateaus in the charging curve. The second temperature plateau is due to the freezing of water. The reason for the first temperature plateau is as follows: it is certain the change in density (density values calculated with respect to the unit of kg/m^3) for 10 to 4 ºC is substantially lower (68.92%) than for 16 to 10 ºC. At the same time, the change in density for 16 to 10 ºC is only 36.75% lower than 22 to 16 ºC. Hence, heat transfer due to the natural convection effect is less in the 10 to 4 ºC region. Meanwhile, for 6 to 4 ºC, the density change is almost negligible. As a result, heat transfer will happen majorly via conduction (conduction resistance is high because thermal conductivity is only 0.6 W/mK) in that region. Due to the combined effect of the two phenomena mentioned above, the rate of decrease in temperature was reduced near 10 to 4 °C and a temperature plateau was observed. After 4 ºC, again, the density change started to increase. Hence, the reduction is happening slightly at a faster rate. The density data were taken from NIST Chemistry WebBook.

Table 6. Onset solidification time without a nucleating agent

Capsule specifications	Delay in onset of solidification (min)	T_w (°C)
BGS, 86 vol%	8.80 to 47.25	-9 (P_n = 1)
D = 64 mm [P.S]	9.50 to 78.20	-6 (P_n = 0.6)
	NS up to 180	-3 (P_n = 0)
BGS [48]**, 80 vol%**		
D = 66 mm	18	-13
D = 128 mm	48	-7.5
BGS [49], **90 vol%**		
D = 62 mm,	20	-7
Cylindrical tank, 100 vol% [50]		
L = 0.85 m W= 1.35 m, H = 0.745 m	30, 60, and NS up to 390	-9, -7, and -5
LDPE sphere [51][52]**,**		
90 vol%, D = 72 mm,	~18.33 and ~20	-12 and -9
Copper cylinder [11]**, 100 vol%**	16.7	-10.5 (P_n =1)

D = 8.28 cm, t = 0.25 cm, L = 14.7 cm,	46.7 NS up to 180	-6 (P_n =0.208) -5 (P_n= 0)
BGB [53], **80 vol%** D = 48 mm,	57.16	-15
SS sphere, [54] **90 vol%** , D = 100 mm D = 86 mm D = 72 mm	 12, 20, and 34 11, 26, and 34 8, 8, and 20	 -12, -9 and -6 -12, -9 and -6 -12, -9 and -6
LDPE sphere, [55] [56], Dia = 68 mm, **80 vol%** **90 vol%**	 ~ 25, ~130, and NA ~ 25, ~ 63 and NS up to 180	 -9, -6, and -3 -9, -6, and -3

LDPE – Low-density polyethylene, BGS – Borosilicate glass sphere, NS – Not Solidified, NA – Not available, SS – Stainless steel, BGB – Borosilicate glass beaker.

3.3. Charging and discharging characteristics of PCM with respect to different sizes of AHC

The experimental results obtained before and after adding the various sizes of AHC (large, medium and small) are presented in **Fig. 6** (a) and (b). **Fig. 6** (a) depicts the charging characteristics of PCM added with large, medium and small sizes of AHC. It is estimated that the CT observed in a 64 mm S.E added with large, medium and small sizes of AHC is 71.30, 62.90 and 59.55 min, respectively, which are 20.86%, 30.19%, and 33.91% lower than that of without AHC. The highest reduction in CT is achieved with the smallest AHC because it has the highest mass of porous materials [57]. **Fig. 6** (a) shows that the CR realised in 64 mm S.E containing large, medium and small sizes of AHC is 8.00, 9.20 and 9.72 W, respectively, which are 24.80%, 43.53% and 51.64% higher than that of without AHC.

Further, the discharging characteristics of PCM added with large, medium and small sizes of AHC are presented in **Fig. 6** (b). It is inferred that the discharging curve is different from the charging curve. The temperature-time history curve sensed by RTD has some fluctuations in the case of discharging, as depicted in **Fig. 6** (b). The constrained melting behaviour [58] can be the reason for such fluctuations in the discharging curve, which can be justified with the help of **Fig. 7**. A separate melting experiment was carried out by keeping S.E in ambient conditions to understand the discharging behaviour of PCM. This discharging experiment was performed without a nucleating agent to visualise the discharging process properly. During this experiment,

the images were captured in subsequent intervals to illustrate the stages of melting. The different stages involved in the constrained melting of ice are represented in **Fig. 7**. In the first stage, after keeping the 64 mm S.E containing ice in ambient condition, the ice started to melt, and the melting progressed eccentrically, as can be affirmed from **Fig. 7**.

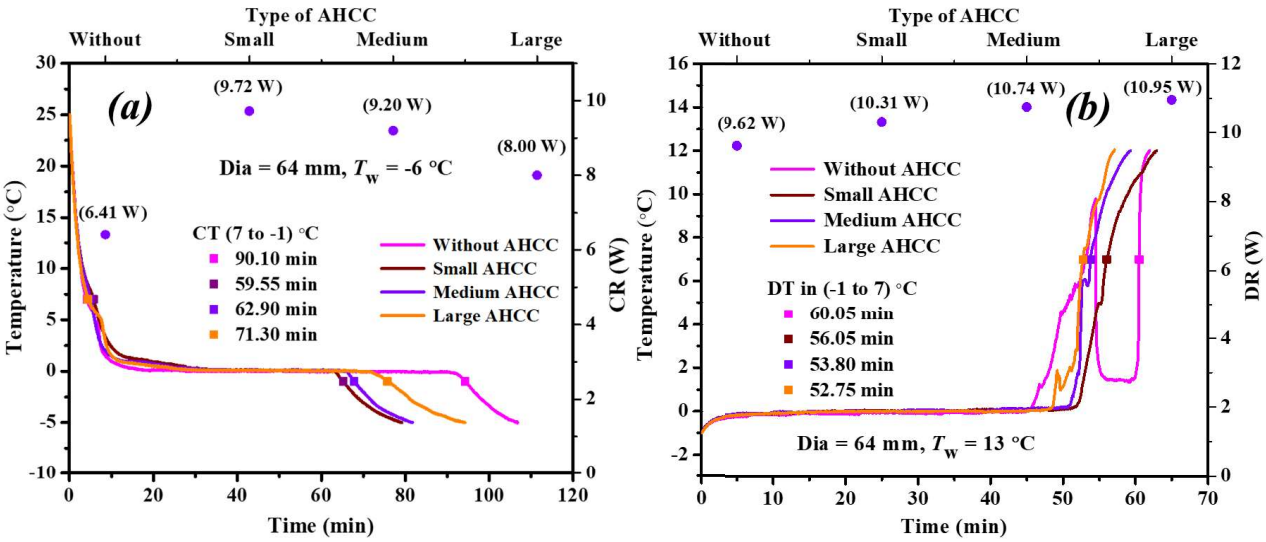

Fig. 6 Influence of various sizes of AHC on (a) Charging characteristics and (b) discharging characteristics of PCM

Furthermore, as the melting progressed, the ice present near the top surface was melted entirely, and the ice near the centre and bottom of S.E remained frozen in the second stage (**Fig. 7**). Due to eccentric melting behaviour, ice was detached from the sensor in the third stage. As a result, a sudden increase in temperature is noted in the PCM's discharging curve (first rise), as shown in **Fig. 6** (b). In the fourth stage, due to the effect of gravity, the ice comes near the sensor again and is attached to the sensor, as can be confirmed in **Fig. 7**. As a result, the temperature suddenly drops (**Fig. 6** (b) (first drop)). In the fifth stage, a small amount of ice remains in contact with the sensor (**Fig. 7**), which is surrounded by higher-temperature water (close to heat transfer fluid temperature). In the final stage, the ice in contact with the sensor melted. Due to this, the sensor suddenly comes in contact with the higher-temperature water, as can be affirmed from **Fig. 7**. As a consequence, the temperature sensed by the sensor rises suddenly (second rise), and it reaches a value close to heat transfer fluid temperature (**Fig. 6** (b)). The discharging curve of AHC does not have significant fluctuations like without AHC. The reason is that the inclusion of AHC arrests the major movement of the ice.

Moreover, from **Fig. 6** (b), it is found that the DT noticed in a 64 mm S.E containing large, medium and small sizes of AHC is 52.75, 53.80, and 56.05 min, respectively, which are 6.61%,

10.41% and 12.16% lower than that of without AHC. Meanwhile, for the same case, the DR realised is 10.31, 10.74 and 10.95 W, respectively, which are 7.17%, 11.64%, and 13.83% greater than those without AHC, respectively. In the case of discharging characteristics, the DT decreases as the size of the AHC increases. Whereas in the case of charging characteristics, an opposite trend is observed, as presented in **Fig. 6 (a)**. Ice is in the centre during the discharging process, and it is surrounded by water, as can be visualised in **Fig. 7**. Therefore, inside S.E, the mode of heat transfer from the water to ice via the S.E surface is influenced more by natural convection rather than conduction. The ice slurry is in the centre during the charging process, and a layer of ice surrounds it. Therefore, the mode of heat transfer between ice slurry and ice via the S.E surface is dominated by conduction rather than natural convection. It is certain that upon increasing the size of AHC (increasing the porosity), the natural convective heat transfer increases, and the conductive heat transfer decreases [29]. Consequently, the DT decreases, and CT increases as the size of AHC increases. **Fig. 8** (a) depicts the 64 mm S.E filled with various sizes of AHC, and **Fig. 8** (b) illustrates the different sizes of AHC.

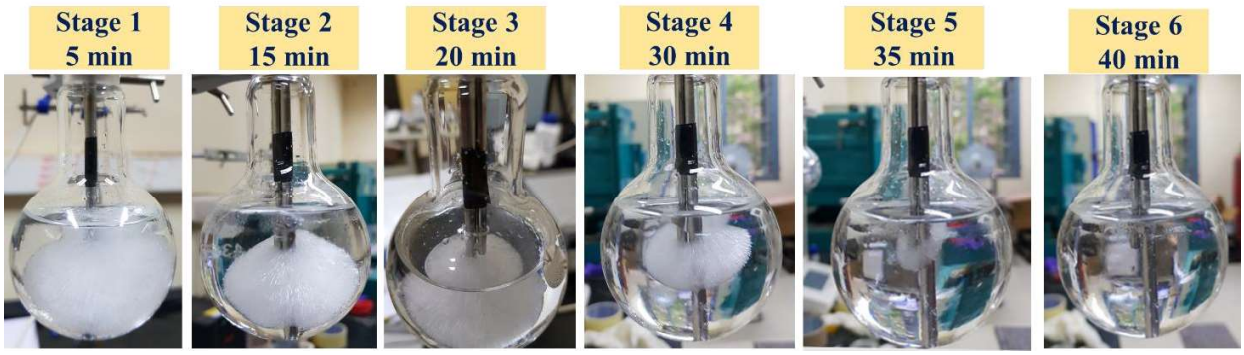

Fig. 7 Different stages in constrained melting behaviour of ice

Furthermore, on the basis of the data illustrated in **Fig. 6** (a), it is intriguing to note that upon decreasing the size of AHC from medium to small and large to medium, the decrease in CT observed is 5.33% and 11.78%, respectively. In addition, **Fig. 6** (b) reveals that upon raising the size of AHC from medium to large and small to medium, the decrease in DT observed is 1.95% and 4.01%, respectively. According to the inferences mentioned above, the reduction in CT is significantly higher while declining the size of AHC from large to medium. Also, the decrease in DT is considerably higher while increasing the size of AHC from small to medium. Therefore, it can be concluded that the medium-size AHC provided effective performance during discharging and charging. Hence, the medium-size AHC is the optimal size AHC. Further study has been carried out using the medium-size AHC, and in the further sections, the word AHC refers to the medium-size AHC.

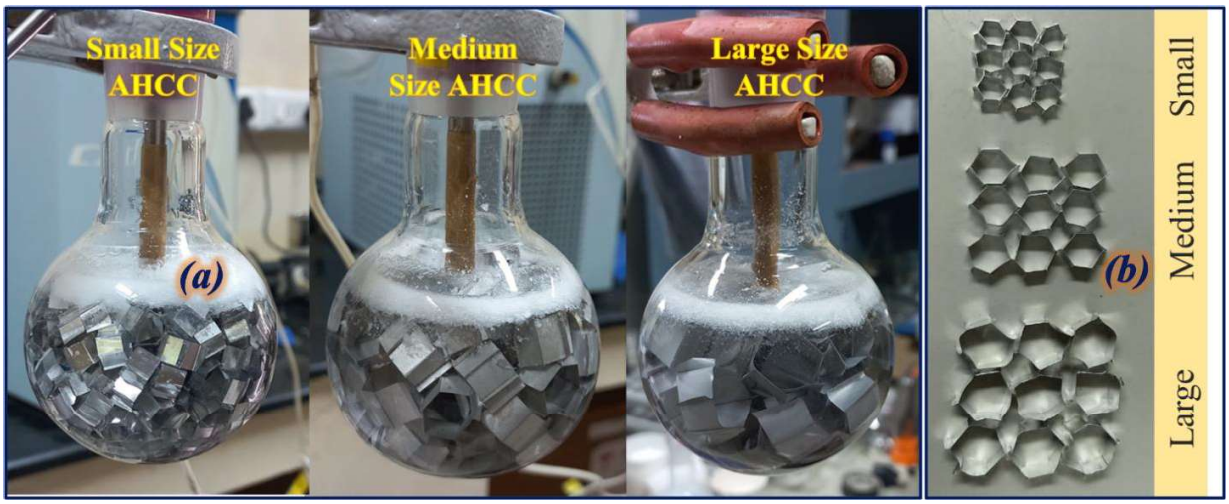

Fig. 8 (a) 64 mm S.E filled with different sizes of AHC and (b) Different sizes of AHC

3.4. Charging characteristics of PCM before and after adding AHC

The experimental results obtained before and after adding AHC are illustrated in **Fig. 9** (a). It is revealed that adding AHC leads to a considerable reduction in CT. The inclusion of AHC inside the PCM leads to the formation of a very stable layered skeleton structure with high thermal conductivity [59], as can be visualised from **Fig. 8**. The presence of a high thermal conductivity stable layer significantly reduces the conductive resistance of PCM and remarkably enhances the effective thermal conductivity of PCM [17,60]. This further leads to a substantial improvement in the CR [25], and it does not have a sedimentation issue. Hence, enhancing the charging characteristics using AHC is economically viable, practically feasible and highly reliable, which subsequently aids in developing an energy-efficacious and sustainable CTSS. The details related to S.E and medium-size AHC are given in **Table 7**.

Furthermore, **Fig. 9** (a) substantiates that after adding AHC, at T_w=-6 °C, the CT observed in 64, 85, and 105 mm S.E is 62.90, 103.50 and 171.40 min, respectively, which are 30.18%, 30.19% and 32.30% lower than that without AHC, as can be seen from **Fig. 9** (a). As a result, after adding AHC, the CR observed in 105, 85 and 64 mm S.E is enhanced by 47.76%, 43.19% and 45.86%, respectively. The inclusion of AHC in PCM enhances the effective thermal conductivity, which would be the possible reason for the decrease in CT and improvement in CR [24]. From the obtained experimental results performed with AHC (**Fig. 9** (b)), it is estimated that the average decrease in CT upon adding AHC is 30.23%, which proves that adding AHC is guaranteed to achieve a 30.23% reduction in chiller working time. As a consequence of this, to store the stated quantity of energy in an S.E filled with AHC, the chiller energy consumption can be reduced by 30.23%.

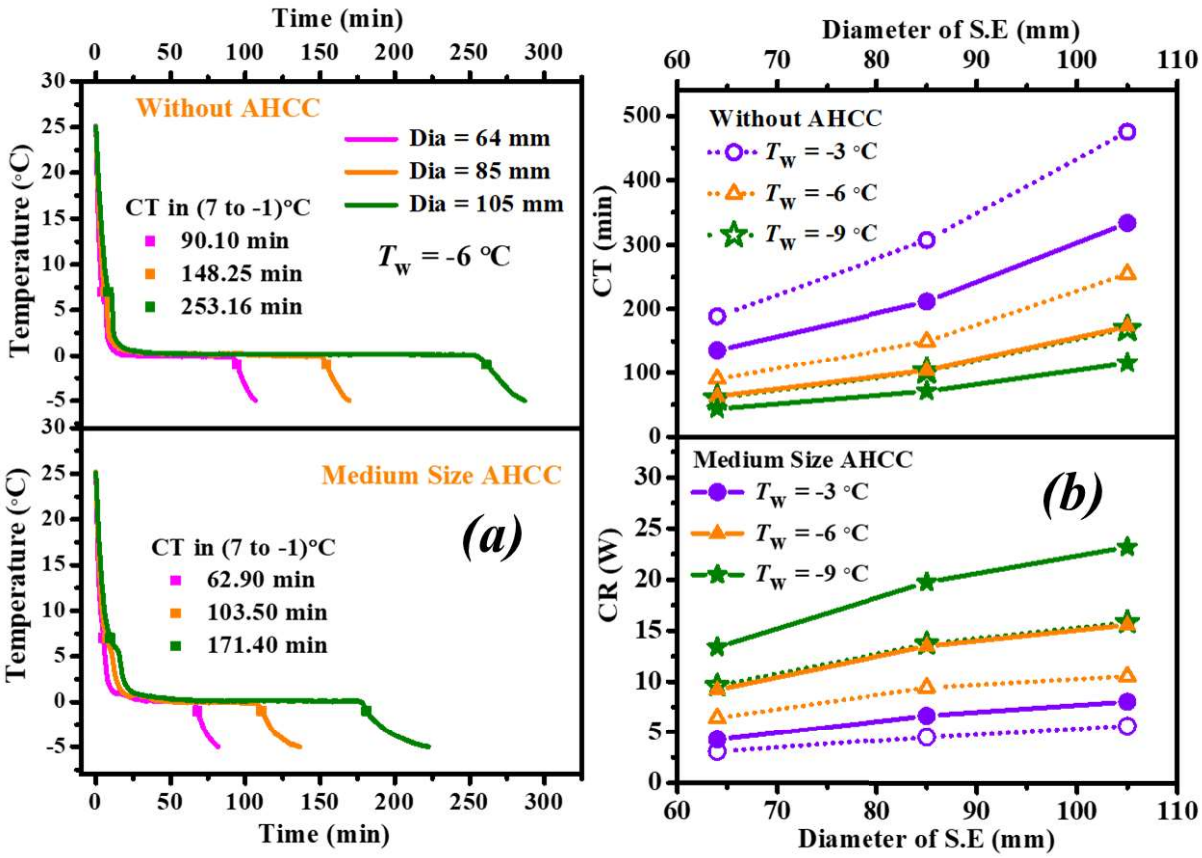

Fig. 9 (a) Charging characteristics of water with and without AHC (b) CR and CT of water with and without AHC

Further, from **Fig. 9** (b), it is interesting to observe that with AHC, the CR and CT obtained in 64, 85, and 105 mm S.E at an optimal heat transfer fluid temperature (T_w=-6 °C) are reasonably close to the CR, and CT realised in the same S.E without AHC at T_w=-9 °C. The results mentioned above reveal that after adding AHC, the charging characteristics realised at T_w=-9 °C can be achieved with AHC at T_w=-6 °C, which is 3 °C greater than that of before adding AHC. Hence, the addition of AHC aids in achieving effective charging characteristics at a higher heat transfer fluid temperature. This would immensely help in enhancing the energy storage efficiency of CTSS. CR and CT noticed in various experiments before and after adding AHC are presented in **Table 8**. From the obtained experimental results (**Fig. 9** (b)), it is calculated that the average decrease in CT and an average improvement in CR realised upon adding AHC are 30.23% and 43.54%, respectively. Hence, utilisation of AHC is guaranteed for storing the energy at a higher CR with lesser specific energy consumption, which is more beneficial for developing a sustainable and energy-efficient CTSS.

Table 7 Medium size AHC and S.E related details

Actual volume of S.E (ml)	Diameter (Outer) of S.E[a] (mm)	Equivalent diameter (outer) based on volume (mm)	Volume occupied by AHC (g)/ Mass of AHC Added (g)	A.M.W.A/ 1-Hexadecanol added (g)	Reduction in ESC (%)
116.00	64.00	62.50	1.76/4.79	95.06/2.94	1.76
280.00	85.00	83.16	4.48/12.24	229.23/7.09	1.86
535.00	105.00	102.71	8.79/24.00	437.77/13.54	1.91

[a] Catalogue specification, ESC – Energy Storage capacity, A.M.W.A – Actual mass of water added.

Table 8 CT and CR realised before and after adding AHC

Dia of S.E	CT (min) Without / With AHC			CR (W) Without / With AHC		
	T_w = -3 °C	T_w = -6 °C	T_w = -9 °C	T_w = -3 °C	T_w = -6 °C	T_w = -9 °C
64 mm	188.63/136.00	90.10/62.90	60.10/43.30	3.06/4.25	6.41/9.20	9.62/13.36
85 mm	306.13/210.35	148.25/103.50	101.87/70.65	4.55/6.63	9.40/13.47	13.67/19.74
105 mm	474.53/332.46	253.16/171.40	168.27/114.90	5.61/8.01	10.51/15.54	15.82/23.18

3.5. Charging characteristics of PCM with AHC in relation to different heat transfer fluid temperatures and diameters

In a 105 mm S.E, at -3, -6 and -9 °C heat transfer fluid temperature, the charging studies were conducted to analyse heat transfer fluid temperature's effect on charging characteristics with AHC. The obtained results are presented in Fig. 10 (a) top graph, which shows that the CT is in a direct relationship with heat transfer fluid temperature [51]. The reason is that the CR increases with a decrease in heat transfer fluid temperature. The obtained CR and CT values are depicted in **Fig. 10** (b). It is deduced that with AHC, the CT decreases, and CR increases upon decreasing the heat transfer fluid temperature. Considering all diameter S.Es filled with AHC (**Table 8**), upon decreasing the heat transfer fluid temperature from -6 to -9 °C and -3 to -6 °C, the average decrease in CT realised is 31.95% and 51.00%, respectively. Meanwhile, the average enhancement in CR is 46.98% and 104.55%, respectively. The results described above ratify that the improvement in CR and decrease in CT achieved by changing the heat transfer fluid temperature from -3 to -6 °C is significantly higher than those realised by changing the heat transfer fluid temperature from -6 to -9 °C [16,38], as illustrated in **Fig. 10** (b). From the above, it is clear that while reducing the heat

transfer fluid temperature up to -6 °C, a higher reduction in charging time and enhancement in charging rate can be achieved.

Further, the Carnot coefficient of performance of the vapour compression refrigeration system (condenser side temperature assumed as 25 °C) for -3, -6 and -9 °C evaporator temperature is 9.64, 8.61, and 7.76, respectively. While reducing the heat transfer fluid temperature from -3 to -6 °C, the reduction in the Carnot coefficient of performance of the chiller is 10.68%. In contrast, the reduction in charging time is found to be 51.00%. At the same time, while reducing the heat transfer fluid temperature from -6 to -9 °C, the reduction in Carnot COEFFICIENT OF PERFORMANCEis 9.85%. In contrast, the reduction in charging time is only 31.95%.

The reduction in the Carnot coefficient of Performance is reasonably equal for -3 to -6 °C and -6 to -9 °C. At the same time, the reduction in charging time is significantly higher in the case of -3 to -6 °C compared to -6 to -9 °C. Moreover, -3 °C is a higher heat transfer fluid temperature, and the coefficient of performance is high (11.95% higher than -6 °C). However, the chiller needs to operate for a longer duration (two times more than -6 °C). On the other hand, -6 °C is a lower heat transfer fluid temperature, and the coefficient of performance will be 10.68% lower than -3 °C. But the chiller can be operated at 51.00% lower time to store the stated amount of energy compared to -3 °C. On the other hand, the reduction in charging realised for -6 to -9 °C is not significantly higher than -3 to -6 °C. Therefore, improving the charging characteristics by declining the heat transfer fluid temperature is highly efficient in the former (-3 to -6 °C) compared to the latter (-6 to -9 °C). On the basis of the results mentioned above, it is substantiated that for all diameter S.Es filled with AHC, the optimal heat transfer fluid temperature required for achieving effective charging characteristics is found to be -6 °C and is therefore proposed as a suitable heat transfer fluid temperature for practical S.E+AHC-based CTSS application.

Further, **Fig. 10** (b) illustrates that CR and CT were noticed in all the experiments performed after adding AHC. It is ratified that the CT increases as the diameter of S.E increases. The reason is that the amount of PCM loaded in S.E increases as the diameter increases. Further, from **Fig. 10** (b), it is revealed that CR increases with the diameter of S.E [38]. Energy stored divided by CT is described as CR. As the size of S.E increases, both the radius and surface area of S.E increase. The increase in the surface area enhances the convective heat transfer prevailing in the wall of S.E. Simultaneously, the increase in radius suppresses the conductive heat transfer (increases conductive resistance). Nevertheless, the increase in conductive resistance is less influential than an increase in convective heat transfer [16]. Hence, CR is in direct relationship with diameter.

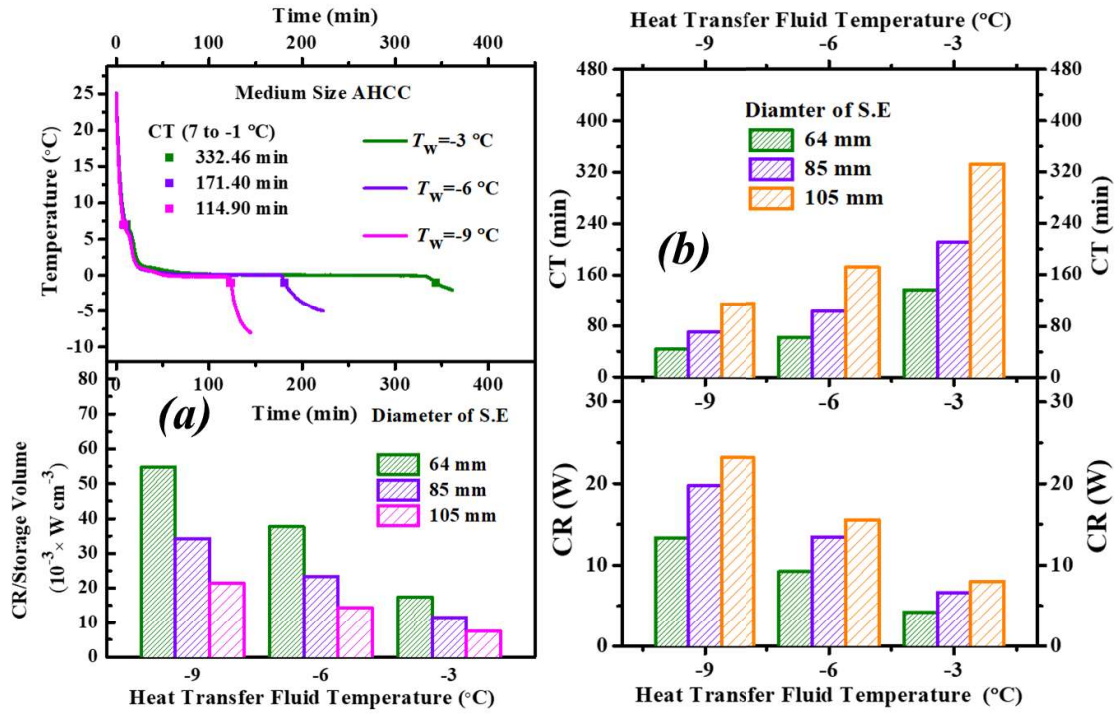

Fig. 10 (a) Charging characteristics of PCM with AHC, (b) Charging characteristics realised at all heat transfer fluid temperatures and all diameters

Furthermore, S.Es are arranged in the storage tank in CTSS. The storage volume occupied by each S.E is reasonably equal to the cubic of its outer diameter, which is 244.14, 575.10 and 1083.52 cm^3 for 64, 85 and 105 mm S.E, respectively. Therefore, exploring the charging characteristics of S.E for a specified storage volume is essential to find a suitable diameter for CTSS. For a specified storage volume, the CR realised at an optimal heat transfer fluid temperature in 105, 85 and 64 mm S.E is 14.34, 23.43 and 37.67 mW cm^{-3}, respectively. It is revealed that CR decreases as the diameter increases for a specified storage volume, as illustrated in **Fig. 10** (a) bottom graph. The same trend has been observed for other heat transfer fluid temperatures. The lowest-diameter capsule delivered the highest CR for a given storage volume. On the basis of the above results, it is substantiated that the lower the diameter, the better the CR for a given storage volume. Hence, among the utilised S.Es, 64 mm is proposed as a suitable S.E for application.

3.6. Discharging characteristics of PCM in relation to different S.E with and without AHC

The discharging characteristics obtained before and after adding AHC are depicted in **Fig. 11** (a) and (b). **Fig. 11** (a) reveals that DT increases as the diameter increases for both cases (with and without AHC). The DT realised in 64, 85, and 105 mm S.E with AHC is 53.80, 80.45, and 108.60 min, respectively **(Table 9)**, which are 10.41%, 11.93% and 9.95% lesser than that of without

AHC, respectively. On the other hand, the DR realised in the same S.Es with AHC is 11.61%, 13.55%, and 11.05% higher than those of without AHC **(Table 9)**. **Fig. 11** (b) shows that DR and DT increase with diameter. Compared to CR and CT, the enhancement in DR and reduction in DT realised are substantially low. The reason is that the AHC addition improves the conductive heat transfer but suppresses the natural convective heat transfer inside S.E [22,29]. As charging is conduction-dominated, AHC plays a predominant role in enhancing the charging characteristics. Hence the reduction in CT is more pronounced. On the other hand, the role of AHC in enhancing the discharging characteristics is not significant because discharging is a natural convection-dominated process. Thus, the enhancement in DR and the decrease in DT realised are less pronounced upon adding AHC.

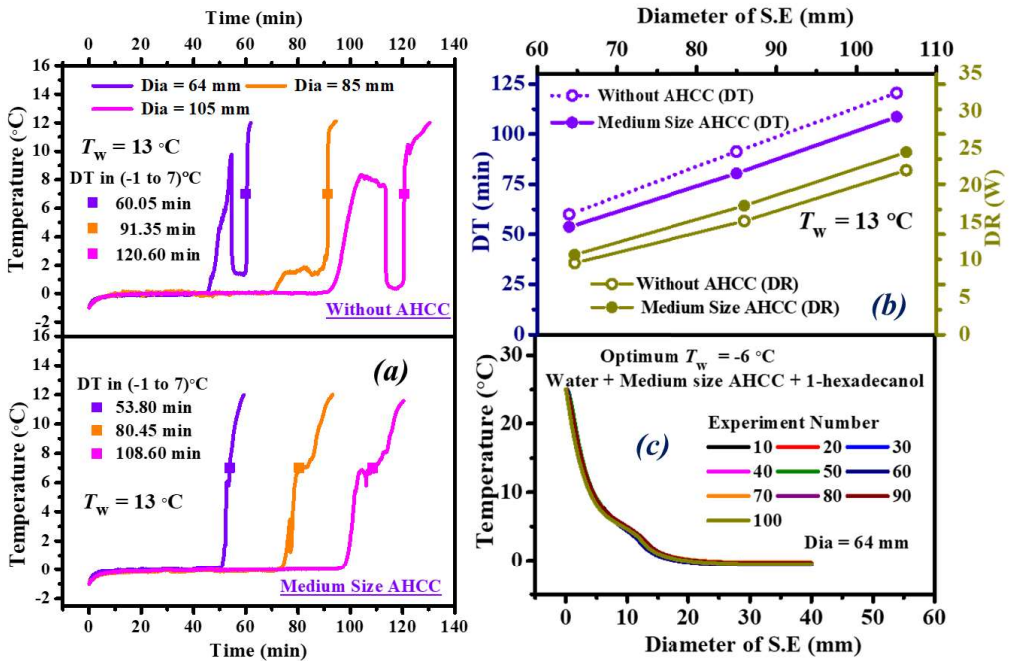

Fig. 11 (a) Discharging characteristics of PCM with and without AHC (b) DR and DT noticed in different diameter S.Es (c) Reliability of 1-Hexadecanol in eliminating the supercooling.

Further, the DR realised in 105, 85 and 64 mm S.E for a given storage volume is 22.62, 30.12, and 43.99 mW cm^{-3}, respectively. It is revealed that the smallest diameter capsule has the highest CR per unit storage volume. Further, DR for a given storage volume decreases as the diameter increases. According to the above results, it is deduced that for a given storage volume, the smaller the diameter better the discharging characteristics. Hence, among the utilised S.Es, 64 mm is proposed as a suitable S.E for application (as concluded in the charging study). In a 64 mm diameter S.E, 100 freezing and melting experiments were performed at an optimal heat transfer

fluid temperature to study the reliability of 1-Hexadecanol in phasing out the supercooling nature of water in the presence of AHC. The freezing curve obtained in every 10th experiment is plotted in **Fig. 11** (c). It is found that supercooling has been eliminated in all the experiments. Hence, it is concluded that 1-Hexadecanol is highly reliable in phasing out the supercooling nature of water.

Table 9 DT and DR realised before and after adding AHC

T_w (°C)	DT (min) Without / With AHC			DR (W) Without / With AHC		
	64 mm	85 mm	105 mm	64 mm	85 mm	105
13	60.05/53.80	91.35/80.45	120.60/108.60	9.62/10.74	15.25/17.32	22.07/24.51

4. Conclusion

In the current study, the supercooling nature of ice was eliminated using a cost-effective nucleating agent (1-Hexadecanol). Further, the energy storage performance of ice was enhanced using the most promising TCE called AHC. From the acquired experimental results, subsequent conclusions have been made.

- After adding 3 wt% 1-Hexadecanol, the supercooling nature of water has been mitigated. This eliminates the idle running time of the chiller and makes the chiller function at a higher evaporator temperature, leading to the effective utilisation of chiller energy.
- The medium size AHC has the potential to deliver optimal performance during charging and discharging. Hence, the optimum size of AHC is found to be medium.
- After adding medium-size AHC, the CT is considerably reduced. The inclusion of AHC leads to a 30.23% reduction in CT. Accordingly, the chiller operating time is reduced by 30.23%.
- Considering all the obtained results, the average improvement in CR upon adding AHC is 43.54%. Upon adding AHC, the average decrease in DT realised is 10.76%. Meanwhile, the DR is enhanced by 12.07%.
- The charging characteristics realised with AHC at -6 °C are reasonably close to that at -9 °C without AHC, proving that adding AHC aids in achieving better-charging characteristics at a higher heat transfer fluid temperature.

- After adding AHC, the optimal heat transfer fluid temperature for charging is -6 °C. Smaller diameter S.E delivered better discharging and charging characteristics for a stated storage volume.
- When the AHC is added with ice, the effective utilisation ratio improved considerably (6.13 to 6.48), and the energy storage capacity reduced slightly (1.76% to 1.91%).

The method adopted to eliminate the supercooling and improve the energy storage performance of ice is economically feasible, practically viable and highly reliable (no sedimentation issue). Upon adding AHC, the energy storage capacity decreased minimally, CR enhanced remarkably, and the effective utilisation ratio enhanced considerably, which will be highly beneficial for application. The above results prove that utilising AHC would pave the way for establishing an energy-efficient and sustainable CTSS. The future study can be focused on developing the numerical model to find the charging performance of water added with AHC. The performance of water in the presence of 1-Hexadecanol and AHC can be tested in different enclosures.

Acknowledgement

We thank the Sophisticated Instrument Facility (SIF), National Institute of Technology, Tiruchirappalli, for providing access to the facility.

References

[1] Qi C, Zhang F, Mu J, Zhang Y, Yu Z. Enhanced mechanical and thermal properties of hollow wood composites filled with phase-change material. J Clean Prod 2020;256:120373. https://doi.org/10.1016/j.jclepro.2020.120373.

[2] Yaxi Li, Chuanchang Li, Niangzhi Lin, Baoshan Xie, Dongyao Zhang JC. Review on tailored phase change behavior of hydrated salt as phase change materials for energy storage. Mater Today Energy 2021. https://doi.org/https://doi.org/10.1016/j.mtener.2021.100866.

[3] Li S-F, Liu Z, Wang X-J. A comprehensive review on positive cold energy storage technologies and applications in air conditioning with phase change materials. Appl Energy 2019;255:113667. https://doi.org/10.1016/j.apenergy.2019.113667.

[4] Sidik NAC, Kean TH, Chow HK, Rajaandra A, Rahman S, Kaur J. Performance enhancement of cold thermal energy storage system using nanofluid phase change

materials: A review. Int Commun Heat Mass Transf 2018;94:85–95. https://doi.org/10.1016/j.icheatmasstransfer.2018.03.024.

[5] Rakkappan SR, Sivan S, Ahmed SN, Naarendharan M, Sai Sudhir P. Preparation, characterisation and energy storage performance study on 1-Decanol-Expanded graphite composite PCM for air-conditioning cold storage system. Int J Refrig 2021;123:91–101. https://doi.org/10.1016/j.ijrefrig.2020.11.004.

[6] Sehar F, Rahman S, Pipattanasomporn M. Impacts of ice storage on electrical energy consumptions in office buildings. Energy Build 2012;51:255–62. https://doi.org/10.1016/j.enbuild.2012.05.002.

[7] Wang X, Dennis M, Jiang J, Zhou L, Zhai X, Lipiński W. Performance of a novel cold thermal storage material in an emulated air conditioning system using different storage strategies. Int J Refrig 2019;104:259–69. https://doi.org/10.1016/j.ijrefrig.2019.05.038.

[8] Christopher S, Parham K, Mosaffa AH, Farid MM, Ma Z, Thakur AK, et al. A critical review on phase change material energy storage systems with cascaded configurations. J Clean Prod 2021;283:124653. https://doi.org/10.1016/j.jclepro.2020.124653.

[9] Yang L, Jin X, Zhang Y, Du K. Recent development on heat transfer and various applications of phase-change materials. J Clean Prod 2021;287:124432. https://doi.org/10.1016/j.jclepro.2020.124432.

[10] Lin X, Zhang X, Ji J, Liu L, Wu Y, Yang M, et al. Development of flexible form-stable phase change material with enhanced electrical resistance for thermal management. J Clean Prod 2021;311:127517. https://doi.org/10.1016/j.jclepro.2021.127517.

[11] Chen SL, Lee TS. A study of supercooling phenomenon and freezing probability of water inside horizontal cylinders. Int J Heat Mass Transf 1998;41:769–83. https://doi.org/10.1016/S0017-9310(97)00134-8.

[12] Chen SL, Wang PP, Lee TS. An experimental investigation of nucleation probability of supercooled water inside cylindrical capsules. Exp Therm Fluid Sci 1998;18:299–306. https://doi.org/10.1016/S0894-1777(98)10040-7.

[13] Lu W, Tassou SA. Characterisation and experimental investigation of phase change materials for chilled food refrigerated cabinet applications. Appl Energy 2013;112:1376–82. https://doi.org/10.1016/j.apenergy.2013.01.071.

[14] Li W, Wang YH, Kong CC. Experimental study on melting/solidification and thermal conductivity enhancement of phase change material inside a sphere. Int Commun Heat Mass Transf 2015;68:276–82. https://doi.org/10.1016/j.icheatmasstransfer.2015.09.004.

[15] Jia X, Zhai X, Cheng X. Thermal performance analysis and optimisation of a spherical PCM capsule with pin-fins for cold storage. Appl Therm Eng 2019;148:929–38. https://doi.org/10.1016/j.applthermaleng.2018.11.105.

[16] Rakkappan SR, Sivan S, Preetham DS, Sudhir PS, Naarendharan M. Facile approach to fend off the supercooling phenomenon of water in a spherical enclosure for energy-efficient and sustainable cold thermal energy storage system. Sustain Energy Technol Assessments 2021;45:101076. https://doi.org/10.1016/j.seta.2021.101076.

[17] Senobar H, Aramesh M, Shabani B. Nanoparticles and metal foams for heat transfer enhancement of phase change materials: A comparative experimental study. J Energy Storage 2020;32:101911. https://doi.org/10.1016/j.est.2020.101911.

[18] Li Z, Gariboldi E. Review on the temperature-dependent thermophysical properties of liquid paraffins and composite phase change materials with metallic porous structures. Mater Today Energy 2021;20. https://doi.org/10.1016/j.mtener.2021.100642.

[19] Wu MQ, Wu S, Cai YF, Wang RZ, Li TX. Form-stable phase change composites: Preparation, performance, and applications for thermal energy conversion, storage and management. Energy Storage Mater 2021;42:380–417. https://doi.org/10.1016/j.ensm.2021.07.019.

[20] Sari A, Karaipekli A. Thermal conductivity and latent heat thermal energy storage characteristics of paraffin/expanded graphite composite as phase change material. Appl Therm Eng 2007;27:1271–7. https://doi.org/10.1016/j.applthermaleng.2006.11.004.

[21] Al-Shannaq R, Farid MM. A novel graphite-PCM composite sphere with enhanced thermo-physical properties. Appl Therm Eng 2018;142:401–9. https://doi.org/10.1016/j.applthermaleng.2018.07.008.

[22] Sardari PT, Grant D, Giddings D, Walker GS, Gillott M. Composite metal foam/PCM energy store design for dwelling space air heating. Energy Convers Manag 2019;201:112151. https://doi.org/10.1016/j.enconman.2019.112151.

[23] Ghasemi Bahraseman H, Languri EM, East J. Fast charging of thermal energy storage

systems enabled by phase change materials mixed with expanded graphite. Int J Heat Mass Transf 2017;109:1052–8. https://doi.org/10.1016/j.ijheatmasstransfer.2017.02.078.

[24] Joshi V, Rathod MK. Experimental and numerical assessments of thermal transport in fins and metal foam infused latent heat thermal energy storage systems: A comparative evaluation. Appl Therm Eng 2020;178:115518. https://doi.org/10.1016/j.applthermaleng.2020.115518.

[25] Yang J, Yang L, Xu C, Du X. Experimental study on enhancement of thermal energy storage with phase-change material. Appl Energy 2016;169:164–76. https://doi.org/10.1016/j.apenergy.2016.02.028.

[26] Xiao X, Zhang P, Li M. Preparation and thermal characterisation of paraffin/metal foam composite phase change material. Appl Energy 2013;112:1357–66. https://doi.org/10.1016/j.apenergy.2013.04.050.

[27] Atal A, Wang Y, Harsha M, Sengupta S. Effect of porosity of conducting matrix on a phase change energy storage device. Int J Heat Mass Transf 2016;93:9–16. https://doi.org/10.1016/j.ijheatmasstransfer.2015.09.033.

[28] Mallow A, Abdelaziz O, Graham S. Thermal charging performance of enhanced phase change material composites for thermal battery design. Int J Therm Sci 2018;127:19–28. https://doi.org/10.1016/j.ijthermalsci.2017.12.027.

[29] Martinelli M, Bentivoglio F, Caron-Soupart A, Couturier R, Fourmigue JF, Marty P. Experimental study of a phase change thermal energy storage with copper foam. Appl Therm Eng 2016;101:247–61. https://doi.org/10.1016/j.applthermaleng.2016.02.095.

[30] Sardari PT, Giddings D, Grant D, Gillott M, Walker GS. Discharge of a composite metal foam/phase change material to air heat exchanger for a domestic thermal storage unit. Renew Energy 2020;148:987–1001. https://doi.org/10.1016/j.renene.2019.10.084.

[31] Rakkappan SR, Sivan S, Raza MA, Relkar A, Mittal H, Adak M. A facile and reliable approach to enhance the energy storage performance of 1-Decanol for sustainable and energy-efficient cold storage system. J Energy Storage 2022;52:104933. https://doi.org/10.1016/j.est.2022.104933.

[32] Rehman T ur, Ali HM, Janjua MM, Sajjad U, Yan WM. A critical review on heat transfer augmentation of phase change materials embedded with porous materials/foams. Int J

Heat Mass Transf 2019;135:649–73. https://doi.org/10.1016/j.ijheatmasstransfer.2019.02.001.

[33] Manyà JJ, Antal MJ, Kinoshita CK, Masutani SM. Specific heat capacity of pure water at 4.0 mpa between 298.15 and 465.65 k. Ind Eng Chem Res 2011;50:6470–84. https://doi.org/10.1021/ie102462g.

[34] Maass O WL. The specific heats and latent heats of fusion of ice and of several organic compounds. J Am Chem Soc 1925;47:1–9. https://doi.org/10.1021/ja01678a001.

[35] Rakkappan SR, Sivan S, Praveen B, Naarendharan M, Sai Sudhir P. Thermal property, charging and discharging characteristics study on tetra-n-butyl ammonium bromide semi-clathrate hydrates for air-conditioning cold storage and secondary refrigerant applications. J Chem Thermodyn 2021;153:106275. https://doi.org/10.1016/j.jct.2020.106275.

[36] Khot S, Sane N, Gawali B. Experimental Investigation of Phase Change Phenomena of Paraffin Wax inside a Capsule. IjettjournalOrg 2011;2:67–71.

[37] Tan FL. Constrained and unconstrained melting inside a sphere. Int Commun Heat Mass Transf 2008;35:466–75. https://doi.org/10.1016/j.icheatmasstransfer.2007.09.008.

[38] Rakkappan SR, Sivan S, Naarendharan M, Sudhir PS, Preetham DS. Experimental Investigation on Enhanced Energy Storage Characteristics of Spherically Encapsulated 1-Decanol/Expanded Graphite Composite for Cold Storage System. J Energy Storage 2021;41:102941. https://doi.org/10.1016/j.est.2021.102941.

[39] Rakkappan SR, Sivan S, Pethurajan V, Aditya A, Mittal H. Preparation and thermal properties of encapsulated 1-Decanol for low- temperature heat transfer fluid application. Colloids Surfaces A Physicochem Eng Asp 2021;614:126167. https://doi.org/10.1016/j.colsurfa.2021.126167.

[40] Gavish M, Popovitz-Biro R, Lahav M, Leiserowitz L. Ice Nucleation by Alcohols Arranged in Monolayers at the Surface of Water Drops. Science (80-) 1990;250:973–5. https://doi.org/10.1126/science.250.4983.973.

[41] Zobrist B, Koop T, Luo BP, Marcolli C, Peter T. Heterogeneous ice nucleation rate coefficient of water droplets coated by a nonadecanol monolayer. J Phys Chem C 2007;111:2149–55. https://doi.org/10.1021/jp066080w.

[42] Zhang Z, Liu XY. Control of ice nucleation: Freezing and antifreeze strategies. Chem Soc

Rev 2018;47:7116–39. https://doi.org/10.1039/c8cs00626a.

[43] Majewski J, Popovitz- Biro R, Bouwman WG, Kjaer K, Als- Nielsen J, Lahav M, et al. The Structural Properties of Uncompressed Crystalline Monolayers of Alcohols CnH2n+1 OH (n = 13–31) on Water and Their Role as Ice Nucleators. Chem – A Eur J 1995;1:304–11. https://doi.org/10.1002/chem.19950010507.

[44] Yinping Z, Yi J. A simple method, the T-history method, of determining the heat of fusion, specific heat and thermal conductivity of phase-change materials. Meas Sci Technol 1999;10:201–5. https://doi.org/10.1088/0957-0233/10/3/015.

[45] Mojiri A, Grbac N, Bourke B, Rosengarten G. D-mannitol for medium temperature thermal energy storage. Sol Energy Mater Sol Cells 2018;176:150–6. https://doi.org/10.1016/j.solmat.2017.11.028.

[46] Hong H, Kim SK, Kim YS. Accuracy improvement of T-history method for measuring heat of fusion of various materials. Int J Refrig 2004;27:360–6. https://doi.org/10.1016/j.ijrefrig.2003.12.006.

[47] Abhat A. Low temperature latent heat thermal energy storage: Heat storage materials. Sol Energy 1983;30:313–32. https://doi.org/10.1016/0038-092X(83)90186-X.

[48] Ismail KAR, Henríquez JR, da Silva TM. A parametric study on ice formation inside a spherical capsule. Int J Therm Sci 2003;42:881–7. https://doi.org/10.1016/S1290-0729(03)00060-7.

[49] Vikram MP, Kumaresan V, Christopher S, Velraj R. Experimental studies on solidification and subcooling characteristics of water-based phase change material (PCM) in a spherical encapsulation for cool thermal energy storage applications. Int J Refrig 2019;100:454–62. https://doi.org/10.1016/j.ijrefrig.2018.11.025.

[50] Huang MC, Chen BR, Hsiao MJ, Chen SL. Application of thermal battery in the ice storage air-conditioning system as a subcooler. Int J Refrig 2007;30:245–53. https://doi.org/10.1016/j.ijrefrig.2006.07.027.

[51] Kumaresan V, Chandrasekaran P, Nanda M, Maini AK, Velraj R. Role of PCM based nanofluids for energy efficient cool thermal storage system. Int J Refrig 2013;36:1641–7. https://doi.org/10.1016/j.ijrefrig.2013.04.010.

[52] Sathishkumar A, Kumaresan V, Velraj R. Solidification characteristics of water based

graphene nanofluid PCM in a spherical capsule for cool thermal energy storage applications. Int J Refrig 2016;66:73–83. https://doi.org/10.1016/j.ijrefrig.2016.01.014.

[53] Liu Y, Liu Y, Hu P, Li X, Gao R, Peng Q, et al. The effects of graphene oxide nanosheets and ultrasonic oscillation on the supercooling and nucleation behavior of nanofluids PCMs. Microfluid Nanofluidics 2014;18:81–9. https://doi.org/10.1007/s10404-014-1411-1.

[54] Chandrasekaran P, Cheralathan M, Velraj R. Influence of the size of spherical capsule on solidification characteristics of DI (deionised water) water for a cool thermal energy storage system - An experimental study. Energy 2015;90:807–13. https://doi.org/10.1016/j.energy.2015.07.113.

[55] Chandrasekaran P, Cheralathan M, Velraj R. Effect of fill volume on solidification characteristics of DI (deionised) water in a spherical capsule - An experimental study. Energy 2015;90:508–15. https://doi.org/10.1016/j.energy.2015.07.086.

[56] Chandrasekaran P, Cheralathan M, Kumaresan V, Velraj R. Enhanced heat transfer characteristics of water based copper oxide nanofluid PCM (phase change material) in a spherical capsule during solidification for energy efficient cool thermal storage system. Energy 2014;72:636–42. https://doi.org/10.1016/j.energy.2014.05.089.

[57] Ebadi S, Tasnim SH, Aliabadi AA, Mahmud S. An experimental investigation of the charging process of thermal energy storage system filled with PCM and metal wire mesh. Appl Therm Eng 2020;174:115266. https://doi.org/10.1016/j.applthermaleng.2020.115266.

[58] Janghel D, Karagadde S, Saha SK. Successive solidification and constrained remelting of n-octadecance in a rectangular enclosure: Experimental and numerical study. Int J Therm Sci 2023;183:107888. https://doi.org/10.1016/j.ijthermalsci.2022.107888.

[59] Wu S, Yan T, Kuai Z, Pan W. Thermal conductivity enhancement on phase change materials for thermal energy storage: A review. Energy Storage Mater 2020;25:251–95. https://doi.org/10.1016/j.ensm.2019.10.010.

[60] Li WQ, Zhang TY, Li BB, Cui FQ, Liu LL. Experimental investigation on combined thermal energy storage and thermoelectric system by using foam/PCM composite. Energy Convers Manag 2021;243. https://doi.org/10.1016/j.enconman.2021.114429.